Distinguishing magmatic zircon from hydrothermal zircon: A case study from the Gidginbung high-sulphidation Au–Ag–(Cu) deposit, SE Australia

Bin Fu [a,*], Terrence P. Mernagh [b], Noriko T. Kita [a], Anthony I.S. Kemp [c], John W. Valley [a]

[a] Department of Geology and Geophysics, University of Wisconsin, Madison, WI 53706, USA
[b] Onshore Energy and Minerals Division, Geoscience Australia, PO Box 378, Canberra, ACT 2601, Australia
[c] School of Earth and Environmental Sciences, James Cook University, Townsville, QLD 4811, Australia

ARTICLE INFO

ABSTRACT

Zircons within the mineralized, silica-pyrite zone of the Gidginbung (Temora) high-sulphidation Au–Ag–(Cu) deposit in the Lachlan Orogen, Australia have been analyzed by both ion microprobe and laser ablation inductively coupled plasma mass spectrometry for titanium and rare earth element (REE) concentrations, as well as their oxygen and hafnium isotopic compositions. These zircons were previously interpreted to be hydrothermal in origin, but the new data are indicative of a magmatic origin. The zircons exhibit chondrite-normalized REE patterns that are characterized by a steep positive slope from La to Lu with a large positive Ce-anomaly and a relatively small negative Eu-anomaly, similar to igneous zircons from the nearby Middledale Gabbroic Diorite and the Boggy Plain Zoned Pluton in the Lachlan Orogen and some hydrothermal zircons from the Mole Granite in the New England Orogen. Apparent temperatures calculated using the Ti-in-zircon thermometer for the Gidginbung zircons are 692° to 782 °C, significantly higher than the inferred ore-forming temperature ($\leq$350 °C) but consistent with magmatic crystallization. The Gidginbung zircons have mantle-like $\delta^{18}O$ values averaging 5.4±0.9‰ VSMOW (2 standard deviations, $n=17$), lower than those from the Barmedman granite (7.6±2.0‰, $n=17$) in the same area. The Gidginbung zircons also have $\varepsilon_{Hf}(t=435$ Ma) values between 6.4±0.9 and 7.8±0.9 (2 standard errors), while the $\varepsilon_{Hf}(t=370$ Ma) for zircons from the Barmedman granite is more variable, ranging from 5.1±1.1 to 8.4±0.8. Consideration of the data from this and previous studies indicates that the zircons in the Gidginbung deposit are indistinguishable from magmatic zircons with regards to their morphology, cathodoluminescence patterns, and chemical and isotopic signatures. The large measured oxygen isotopic fractionation between quartz and zircon (average: ~10‰) indicates that the minerals did not form by the same process and/or from the same reservoir at $T\geq$350 °C. While most inclusions in zircon are interpreted to have been trapped after zircon formation or resorption, it is possible that, like quartz, rutile, and anatase, a few pyrite inclusions occurring wholly within zircons have formed at relatively high temperatures during zircon crystallization in magma. Thus, the U–Pb age of these zircons (436 Ma) represents the igneous crystallization age and the Gidginbung zircons investigated by us are best interpreted as magmatic relicts of the earliest Silurian igneous rocks, which survived the processes of hydrothermal alteration and mineralization.

© 2008 Elsevier B.V. All rights reserved.

1. Introduction

In the past two decades, zircons have been reported in hydrothermal alteration and/or Au mineralization from many localities and interpreted to be hydrothermal in origin (e.g., Rubin et al., 1989; Claoue-Long et al., 1990; Corfu and Davis, 1991; Claoue-Long et al., 1992; Rubin et al., 1993; Kerrich and King, 1993; Kerrich and Kyser, 1994; Ramezani et al., 2000; Hu et al., 2004; Hoskin, 2005; Pettke et al., 2005; Kebede et al., 2007; Pelleter et al., 2007). These so-called hydrothermal zircons are believed to precipitate from aqueous fluids, in most cases at relatively low temperatures, rather than from magmas.

Hoskin and Schaltegger (2003) have summarized both textural and compositional characteristics of hydrothermal zircons in the literature, and they conclude that the characteristics are not definitive; hydrothermal zircons may be zoned or unzoned; spongy in texture; anhedral or faceted in morphology; and either high or low in common-Pb. In addition, light rare earth element (LREE) abundances may differ from associated magmatic zircons (e.g., Hoskin, 2005; Pettke et al., 2005). Because zircon commonly crystallizes in magmas (or in high-grade metamorphic rocks and anatectic melts), the distinction between magmatic, metamorphic, and hydrothermal zircons is crucial for understanding the behavior of zircon in hydrothermal fluids, in magmatic-hydrothermal processes and for interpreting U–Pb ages.

Recently, Lawrie et al. (2007) reported the presence of zircons, *all* thought to be of hydrothermal origin, in the Gidginbung (Temora) Au–Ag–(Cu) deposit from the Lachlan Orogen in southeastern Australia.

* Corresponding author. School of Earth Sciences, The University of Melbourne, Parkville, VIC 3010, Australia. Fax: +61 3 8344 7761.
E-mail address: binfu@unimelb.edu.au (B. Fu).

Lawrie et al. (2007) suggested four main lines of evidence for the hydrothermal origin of these zircons: (1) the Gidginbung zircons coexist with sulphides and alteration minerals within main ore zones; (2) some of the Gidginbung zircons may contain biphase aqueous inclusions of unknown salinity with homogenization temperatures from ~310° to 340 °C; (3) the Gidginbung zircons apparently contain inclusions of pyrite and strengite [$Fe(PO_4) \cdot 2H_2O$], identified by laser Raman microprobe; and (4) the zircons display trace element (in particular, As and Sb) zonation patterns. Therefore, Lawrie et al. (2007) proposed that the U–Pb age of 436 Ma for zircons analyzed by SHRIMP (Sensitive High Resolution Ion Micro-Probe) from the main ore zone should represent the timing of gold mineralization.

The current study is aimed at better characterizing these zircons and constraining their origins. Laser ablation inductively coupled plasma mass spectrometry (LA-ICP-MS) and ion microprobe/SIMS (secondary ion mass spectrometry) have been employed to measure isotopic (O, Hf) and trace element (Ti, REE) compositions of the zircons. These new chemical and isotopic results allow us to determine whether the zircons are hydrothermal or magmatic in origin and to further constrain the timing of Au–Ag–(Cu) mineralization at Gidginbung.

2. Regional geology

The Lachlan Orogen in southeastern Australia consists of complexly deformed early Palaeozoic volcanic, volcaniclastic and sedimentary rocks extensively intruded by a series of Silurian to Middle Devonian granitic plutons (e.g., Gray and Foster, 2004). The Wagga Group to the west of the Gilmore Fault (Fig. 1) consists of a sequence of deep-water, metasedimentary rocks of Late Ordovician age (Duggan and Lyons, 1999). The Gilmore Fault is a major boundary between metasedimentary rocks and peraluminous granites to the west and a complex sequence of Ordovician to Devonian sedimentary and volcanic rocks, intruded by metaluminous and peralkaline granites to the east (e.g., Wormald and Price, 1988).

The Gidginbung deposit occurs in a poorly exposed intermediate volcanic complex within the West Wyalong—Junee area, part of the Junee—Narromine Volcanic Belt in the Ordovician—earliest Silurian Macquarie Arc (e.g., Glen et al., 2007a). Andesitic lavas and tuffs dominate the sequence, and basaltic andesites and latites are also present. The Gidginbung Volcanics (and Belimebung Volcanics) occur as a wedge of material between the higher grade rocks of the Wagga-Omeo Metamorphic Belt and Silurian Combaning Formation sediments, which lie mainly to the east of the Booberoi Fault (Fig. 1; Bacchin et al., 1999). The Combaning Formation is a monotonous sequence of siltstones, phyllites, sandstones, carbonaceous siltstones and cherts, overlain by micaceous sediments (Warren et al., 1995). These sediments also cover the Springdale Rift, which is interpreted as a northerly trending half-graben that is fault bounded on the western margin and hinged on the eastern margin (Bacchin et al., 1999). The Frampton Volcanics crop out to the southeast as a sequence of predominantly dacitic to rhyolitic tuffs (Warren et al., 1995).

Several Devonian granitic and dioritic intrusions occurring to the east of the Gilmore Fault have been well documented for better understanding of magmatism and crustal growth (e.g., Wormald et al., 2004; Kemp et al., 2005a). Magmatic zircons from these intrusions in the same area are selected for comparison with zircons from the Gidginbung gold deposit. The Middledale Gabbroic Diorite intrudes the Combaning Formation just to the east of the Springdale Rift (Fig. 1). It is composed dominantly of labradoritic plagioclase and brown pargasitic hornblende (partially replaced by chlorite). All original augite and hypersthene appear to have been replaced by secondary amphibole. Hematite, ilmenite and lesser amounts of magnetite are also present. Two zircon standards named Temora-1 and Temora-2, separated from boulders in the northern margin of the Middledale Gabbroic Diorite stock, were dated at 416.8±2.2 Ma (2SD) and 416.8± 2.6 Ma (2SD) by isotope dilution thermal ionization mass spectro-

metry (ID-TIMS; Black et al., 2003a,b, 2004). The zircon is present as coarse grains (≤600 μm) and sector zoning is common.

The late Devonian Narraburra Complex contains three granitic suites, two of which (Narraburra and Barmedman) outcrop to the north of the Gidginbung deposit (Fig. 1). Granites of the Narraburra Suite are peralkaline and vary from medium-grained rocks containing ferrohedenbergite, aegirine–augite, fayalite, and zoned alkali amphiboles to more evolved, coarse-grained hypersolvus granites with aegirine and arfvedsonite–riebeckite amphiboles and albitized feldspars (Wormald et al., 2004). Despite having an elevated whole-rock Zr content (239–799 ppm; Wormald et al., 2004), the zircons are only common where amphibole rather than pyroxene is the dominant mafic phase (Kemp et al., 2005a). Large (≤600 μm), inclusion-free, irregular to euhedral zircons have been obtained from the Narraburra Suite and dated at 375±8 Ma (2SD) (Kemp et al., 2005a).

The Barmedman Suite is metaluminous to weakly peraluminous and comprises pink biotite±hornblende granites that contain fayalite and are characterized by Rapakivi texture (Kemp et al., 2005a). The biotite is usually red-brown, which is more typical of S-type granites as is the associated tin mineralization. Zircons of the Barmedman granite are euhedral and exhibit intricate oscillatory zoning. They are morphologically more variable than those of the Narraburra Suite with both short prismatic and elongate crystals. Some grains have rounded cores with truncated zoning (Kemp et al., 2005a). The Barmedman zircons yielded a SHRIMP U–Pb age of 370±2.4 Ma (2SD, n=41; L.P. Black, Geoscience Australia, unpublished data; Electronic Annex Table EA1), which indicates that the Barmedman Suite formed in the Late Devonian.

3. Gidginbung Au–Ag–(Cu) deposit

The Gidginbung deposit (past production 21t Au) is a high-sulphidation Au–Ag–(Cu) deposit (Allibone et al., 1995) characterized by advanced argillic alteration and associated with andesites and volcanic rocks of Late Ordovician age (e.g., Cooke et al., 2007, and references therein). Hough et al. (2007) further regarded it, together with Peak Hill, as being a porphyry (or porphyry-related) Cu–Au deposit. Porphyries in the region were emplaced during the ~50 million year punctuated history of the earliest Ordovician to earliest Silurian intra-oceanic Macquarie Arc (Glen et al., 2007b). Typical porphyry deposits in the Cadia district were dated at early Late Ordovician and Early Silurian (Wilson et al., 2007).

The orebody is hosted in a relatively gently dipping sequence of interbedded epiclastic breccias and mudstones (Lawrie et al., 1997a). The breccias are interbedded with thin (<2 m thick) beds of fine-grained, finely-laminated mudstones. They are polylithic, multi-phase breccias, with dominantly epiclastic lithologies. Clasts vary enormously in size, with individual blocks up to 40 m in length.

The host rocks are largely undeformed with intense development of penetrative cleavage restricted to within relatively minor shear zones less than 2 m wide (Lawrie et al., 1997b). This localized shearing and cataclastic re-brecciation occurs only rarely, along the margins of larger silicified clasts and alteration zones (Lawrie et al., 1997a,b). The deposit has undergone pervasive hydrothermal alteration and massive sulphide mineralization with tubular geometry, and an inner intensely altered and mineralized silica-pyrite core. Copper mineralization typically forms a concentric shell around the gold mineralization indicating deposition at lower temperatures, but pods of high-grade gold and copper mineralization also occur below the base of the oxidized zone.

Three petrographically distinct igneous rocks occur in the vicinity of the Gidginbung deposit (Allibone et al., 1995). The most common rock type contains pseudomorphs of amphibole phenocrysts and partially replaced plagioclase phenocrysts. Relict accessory phases include titanomagnetite, zircon and apatite. A less common, plagioclase porphyritic rock is distinguished by its lack of amphibole phenocrysts
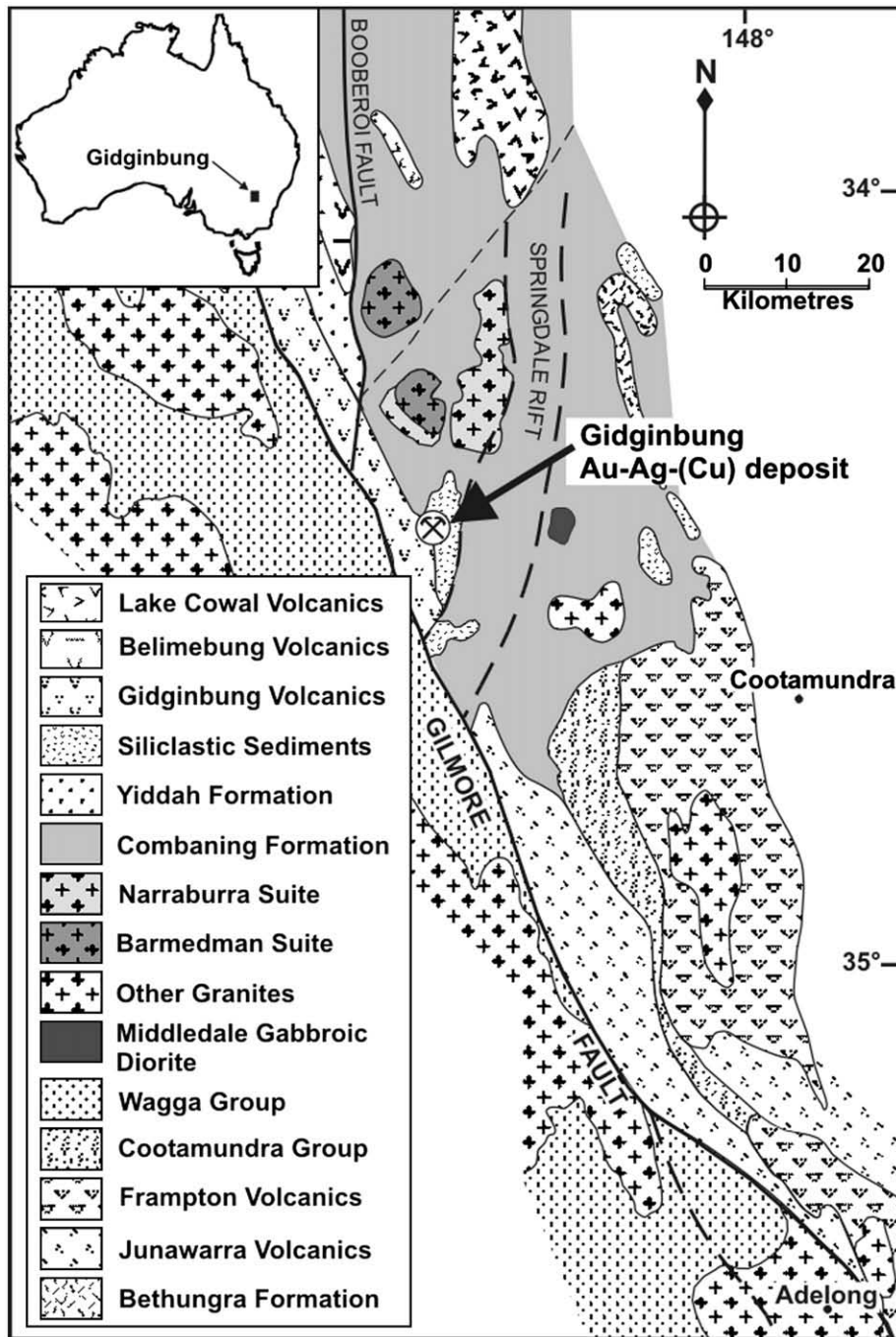
Fig. 1. A simplified geological map of the West Wyalong–Temora–Adelong district in New South Wales, Australia (after Lawrie et al., 2007). Note that the Cootamundra Group contains minor sediments and abundant felsic volcanics (including the Cowcumbala rhyolite).

and presence of scattered relict biotite phenocrysts. The distribution of plagioclase-biotite porphyritic rock suggests that it represents a shallow-level intrusion, which cuts the adjacent plagioclase-amphibole intrusive rock. Steeply dipping tabular bodies of sparsely porphyritic latite or dacite also occur in the vicinity of the open pit. Magmatic zircons from one of these latite or dacite bodies in the vicinity of the Gidginbung deposit yielded a mean $^{206}Pb/^{238}U$ age of 435.0±5.0 Ma (2SD; Perkins et al., 1995).

The exact timing of the gold mineralization at Gidginbung has been controversial. The gold deposit was thought to have formed at ~420 to 400 Ma based on previously published, rather inconsistent K–Ar ages of alunite and highly discordant $^{40}Ar/^{39}Ar$ age spectra of illite (Perkins et al., 1995; Jaques et al., 2002). However, SHRIMP U–Pb analyses of zircons from the high Au-grade silica–pyrite zone in the centre of the Gidginbung deposit gave a weighted mean $^{206}Pb/^{238}U$ age of 436±6 Ma (2SD; Electronic Annex Table EA1), which was interpreted to represent the age of gold mineralization (Lawrie et al., 2007), indistinguishable from the age of neighboring latite or dacite bodies as mentioned above. The close agreement between the age of the igneous rocks and the age of mineralization interpreted by Lawrie et al. (2007) is in accord with studies of other porphyry-epithermal districts which indicate that mineralization occurs within a few million years after intrusion of the igneous source rocks (e.g., Gustafson et al., 2001).

Lawrie et al. (2007) reported that the zircons at Gidginbung commonly occur with rutile, barite, pyrophyllite, quartz, pyrite and enargite in veins and vein selvages. They are generally coarse, mostly

from 200–500 μm in size, and euhedral to subhedral in shape. As shown in Electronic Annex Fig. EA1, zircons from the Gidginbung deposit display well developed growth zoning (oscillatory or sector zoned), identified by cathodoluminescence (CL) imaging. As concluded by Lawrie et al. (2007), the zircons from Gidginbung have the same textural characteristics as contemporaneous magmatic zircons from dykes, minor porphyry intrusions and coarse-grained larger intrusions in the same volcanic belt. However, some of the Gidginbung zircons also contain inclusions of pyrite, strengite, quartz, rutile, anatase, titanite, barite and (chlor-)apatite (Lawrie et al., 2007), which have not been reported in magmatic zircons from elsewhere in the region.

4. Sample preparations and analytical techniques

Two samples of the silica-pyrite rock in the inner mineralized zone of Gidginbung Au–Ag–(Cu) deposit and Barmedman granite (Table 1) were previously collected and two zircon mounts were prepared by Lawrie et al. (2007). Both rock samples were crushed, and the zircons were concentrated at Geoscience Australia, Canberra by standard crushing, gravity and magnetic separation techniques, and then hand-picked under binocular microscope. Cathodoluminescence images of the zircons were previously obtained with a Hitachi S2250-N scanning electron microscope at the Australian National University, Canberra (Electronic Annex Fig. EA1; Lawrie et al., 2007).

4.1. LA-ICP-MS

Trace elements have been analyzed by a UV laser ablation microprobe coupled to an Agilent HP7500 ICP-MS at the GEMOC ARC National Key Centre, Macquarie University, Sydney. Detailed descriptions of instrumentation and analytical and calibration procedures are given by Norman et al. (1996, 1998). The laser ablation system is a Merchantek 213 nm laser coupled to a NewWave Research microscope. Most of the analyses were done with a pulse rate of 5 Hz, using 13% Iris and 100% power output, and a beam energy of 0.1 mJ per pulse, achieving spatial resolution of 20–30 μm. Quantitative results for 32 elements were obtained through calibration of relative element sensitivities using the NIST-610 standard glass, and normalization of each analysis to the electron microprobe data for Hf as an internal standard.

Samples were analyzed in separate runs comprising 10 analyses of unknowns bracketed before and after by 2 analyses of the NIST 610 standard glass. The BCR2G basaltic glass was also analyzed during each run as an independent control on reproducibility and instrument stability. The precision and accuracy of the NIST 610 analyses are better than 1–2% for REE, Y, Sr, Nb, Ta, Hf, Th and U, and from 2 to 5% for Mn, P, Fe, Co, Ni, Cu and Zn. All laser ablation ICP-MS analyses were made on transparent regions of zircon and attempted to avoid any solid inclusions in the zircons, however, some microinclusions may have been included in the analyses due to the relatively large diameter of the laser beam (~30 μm).

The hafnium isotope compositions of zircons were measured at the University of Bristol using a ThermoFinnigan Neptune MC-ICP-MS attached to a New Wave 193 nm laser sampling system. Analytical routines are as described by Kemp et al. (2005a, 2006a). Analyses were conducted over 60 s using a 40 μm beam size and 4 Hz laser repetition rate, with a laser fluence of 6–7 J/cm². Wherever possible, the 10 μm pits generated by the foregoing oxygen isotope analysis were targeted, although this proved impractical for thin zircon rims. A number of secondary zircon standards (QGNG, Temora-2 and FC1) were analyzed throughout the session as a monitor of data quality. Average measured $^{176}Hf/^{177}Hf$ ratios at 2 standard deviations were 0.281609 ± 16 for QGNG ($n=8$), 0.282687 ± 14 for Temora-2 ($n=8$) and 0.282177 ± 24 for FC1 ($n=16$), identical to the solution Hf values for these zircons quoted by Woodhead and Hergt (2005).

Table 1
Oxygen isotopic composition of zircons from the Gidginbung Au–Ag–(Cu) deposit and, for comparison, other igneous rocks from the Lachlan Orogen, Australia

Suite/Pluton	Sample	Location	Latitude	Longitude	Description	$\delta^{18}O$ (Zrc) ‰	Data sources	$\delta^{18}O$ (Zrc)±2SD, ‰	Data sources	U–Pb Age±2SD, Ma	Data sources
	8501001	Gidginbung Au deposit	34°19'40"S	147°27'32"E	High Au-grade silica-pyrite zone	4.22 to 6.02 (n=17)	(1)	5.37±0.93 (n=17)	(1)	436±6	(5)
Barmedman Suite	98844518	Barmedman	34°10'09"S	147°30'14"E	Tourmaline–biotite–granite	5.95 to 9.60 (n=17)	(1)	7.64±2.00 (n=17)	(1)	370.0±2.4	(6)
Narraburra Suite		Narraburra	34°20'11"S#	147°39'02"E#	Peralkaline granite					375±8	(9)
	Temora-1	Middledale	34°20'15"S	147°44'37"E	Gabbroic diorite	7.89 to 7.96 (n=3)ᵃ	(2)	7.93±0.07 (n=3)ᵃ	(2)	416.8±2.2ᵇ	(7), (8)
	Temora-2	Middledale	s.a.a.	s.a.a.	Gabbroic diorite	8.19 to 8.21 (n=3)ᵃ	(2)	8.20±0.02 (n=3)ᵃ	(2)	416.8±2.6ᵇ	(7), (8)
	Temora-2	Middledale	s.a.a.	s.a.a.	Gabbroic diorite	7.74 to 8.67 (n=23)	(3)	8.27±0.40 (n=23)	(3)		
	B4-28	Blind	36°36'02"S#	148°45'11"E#	Gabbro	5.51, 6.33 to 7.25 (n=13)	(3)	6.69±0.92 (n=13)	(3)	~417	(10)
Why Worry Suite	TKB100	Why Worry	36°52'44'S#	149°37'42'E#	Tonalite	6.80 to 9.41 (n=15)	(3), (4)	8.10±1.47 (n=15)	(3), (4)	393.0±5.2	(4)
Why Worry Suite	TKB17	Pretty Point	s.a.a.	s.a.a.	Tonalite	7.01 to 9.12 (n=18)	(3), (4)	8.13±1.29 (n=18)	(3), (4)	401.2±10.6	(4)
Why Worry Suite	TKB15	Why Worry	s.a.a.	s.a.a.	Syn-plutonic basalt (enclave)	5.82 to 7.36 (n=7)	(3), (4)	6.82±1.20 (n=7)	(3), (4)	397.5±9.2	(4)
Cobargo Suite	TKB11	Cobargo	36°23'15"S#	149°53'16"E#	(monzo-) granite	5.53 to 7.60, 9.40 (n=25)	(3), (4)	6.50±1.49 (n=25)	(3), (4)	385.2±5.2	(4)
Cobargo Suite	TKB1	Cobargo	s.a.a.	s.a.a.	Tonalite (or quartz diorite)	5.84 to 7.13, 8.60 (n=21)	(3), (4)	6.52±1.22 (n=21)	(3), (4)	389.3±5.0	(4)
Cobargo Suite	TKB5	Cobargo	s.a.a.	s.a.a.	Diorite (or enclave)	5.66 to 7.09, 7.91 (n=20)	(3), (4)	6.70±0.95 (n=20)	(3), (4)	387.9±8.6	(4)
Jindabyne Suite	KK2	Round Flat	36° 13' 22" S#	148° 39' 33" E#	Tonalite	6.38 to 9.42 (n=11)	(3), (4)	7.74±2.19 (n=11)	(3), (4)	416.4±11.8	(4)
Jindabyne Suite	KK4	Round Flat	s.a.a.	s.a.a.	Tonalite	4.81, 5.92 to 7.93, 9.08 (n=14)	(3), (4)	6.87±1.97 (n=14)	(3), (4)	415.5±14.4	(4)

Data sources: (1) this study; (2) Black et al. (2004); (3) Kemp et al. (2007); (4) Black et al. (2003a); (8) Black et al. (2003b); (9) Kemp et al. (2005a,b); (5) Lawrie et al. (2007); (6) L.P. Black, Geoscience Australia, unpublished data; (7) Black et al. (2003a); (8) Black et al. (2003b); (9) Kemp et al. (2005a); (10) W.J. Collins, pers. comm.
#The latitude and longitude of intrusions were approximately estimated based on geological maps (Hine et al., 1978; Kemp et al. 2005a,b) and Google Earth 4.3 Beta (http://earth.google.com).
ᵃ By laser fluorination; others by SIMS.
ᵇ By ID-TIMS; others by SHRIMP. Zrc: zircon; s.a.a.: same as above.

4.2. Ion microprobe

Ion microprobe analyses of $^{18}O/^{16}O$ ratios and trace element (Ti and REE) concentrations in zircons, correlated with the U–Pb analysis spots if applicable, were made on a CAMECA IMS-1280 secondary ion mass spectrometer at the University of Wisconsin, Madison. The analysis conditions and procedure of data reduction are described by Page et al. (2007a,b).

For oxygen isotope analysis, the Cs^+ beam was focused to a diameter of ~ 10 µm on the sample surface, two Faraday cup detectors were used to measure ^{16}O and ^{18}O simultaneously. Sample analyses were bracketed by 11 or 12 spot analyses on the KIM-5 zircon standard (Valley, 2003) and no drift corrections were made. The spot to spot precision of $^{18}O/^{16}O$ ratio for multiple spots on KIM-5 yielded much better than 0.72‰ (2 SD). Rare earth elements, Y, Hf and Ti were measured by spot analysis on the zircons of interest. NIST 610 glass was used as a calibration standard for trace elements, and zircon standards 91500 and KIM-5 were analyzed as running references. The ^{160}Gd value was corrected, due to interference of ^{160}Dy, using the equation: (^{160}Gd) corrected $= (^{160}Gd)$ measured $- (^{163}Dy)$ measured $\times (2.34/24.9)$. Correction factors of 1.25 for Y, REEs, and Hf, and 1.11 for Ti, were applied to relative sensitivity factors (RSF) of zircon from those of NIST 610 glass, based on the difference in RSF between NIST 610 and zircon standards (zircon 91500 for Y, REE and Hf, and synthetic Ti-doped zircon, made by E. B. Watson, for Ti; Page et al., 2007a).

5. Results

5.1. Zircon chemistry and Ti-in-zircon thermometry

Trace element concentrations in zircon from the Gidginbung deposit were determined by LA-ICP-MS, and the results are tabulated in Electronic Annex Table EA2: Zircons from the Gidginbung deposit have relatively low concentrations of Ti, Ga, Mn and P. Iron concentrations are generally below the ~ 23 ppm detection limit of LA-ICP-MS. Arsenic concentrations in zircons from Gidginbung ranged from 15 to 64 ppm (for PIXE data, see Lawrie et al., 2007). To our knowledge, there are no arsenic data available for either igneous or hydrothermal zircons elsewhere in the literature for comparison.

REE abundances of zircons from Gidginbung, analyzed by both LA-ICP-MS and SIMS, were normalized to C1-chondrite values (McDonough and Sun, 1995) and plotted on log_{10} versus element (La–Lu) diagrams (Fig. 2). The chondrite-normalized REE patterns of zircons from Gid-ginbung are characterized by a steep positive slope from La to Lu with a significantly positive Ce-anomaly and relatively small negative Eu-anomaly. One zircon (#10B) is enriched in As and Yb in the rim (Electronic Annex Fig. EA3), and it has the lowest $(Sm/La)_N$ and $(Ce/Ce^*)_N$ $(=(Ce)_N/SQRT(La\cdot Pr)_N)$ values (Electronic Annex Table EA2).

Both SIMS and LA-ICP-MS gave a large range of titanium concentrations in one zircon grain (#210) from Gidginbung (Electronic Annex Table EA2): 8.1 to 16 ppm (11.6±6.3, 2SD, n=5), SIMS; 5.6 to 15 ppm (8.5±5.6, 2SD, n=10), LA-ICP-MS. The large spot to spot variability is seen by both techniques and we attribute these differences to heterogeneity. Apparent Ti-in-zircon temperatures ranging from 692° to 782 °C (724±52 °C, 2SD, n=10, by LA-ICP-MS; or 752±50 °C, n=5, by SIMS) were estimated based on the calibration of Watson and Harrison (2005) and Watson et al. (2006), which assumes that zircons crystallized in the presence of quartz and rutile at $P \approx 10$ kbar.

The pressure correction for the Ti-in-zircon thermometer is approximately 50 °C/10 kbar at 750 °C for most crustal materials: ~ −50 °C at 1 bar (Ferry and Watson, 2007). Considering the fact that both quartz and rutile are present in the silica-pyrite rock from the Gidginbung deposit, all the Ti-in-zircon temperatures reported above should be ~ 50 °C lower after pressure correction (1 bar), 640–730 °C, which is significantly higher than the ore formation temperature (275°–340 °C) estimated from alteration assemblages at Gidginbung (Allibone et al., 1995), but comparable to that for typical magmatic zircons in mafic to felsic rocks (Fu et al., 2008). A survey of 484 igneous zircons from intrusions or volcanic rocks, kimberlites, and metasedimentary rocks of varying geological age by Fu et al. (2008) indicates that most of the zircons have Ti concentrations of less than 20 ppm, and that apparent Ti-in-zircon temperatures (mostly between ~ 600° and 850 °C) are lower than either zircon saturation temperatures for granitic rocks or predicted crystallization temperatures (> 15% melt residue) for mafic rocks. These surprisingly low temperatures cannot be attributed to any single factor, such as: activities of SiO_2 and TiO_2, effect of pressure, subsolidus resetting of Ti compositions, non-Henry's Law substitution of Ti in zircon, disequilibrium crystallization from melts, or growth of zircons in late melts with evolved hydrous composition. Thus, the Ti-in-zircon thermometer may actually underestimate true crystallization temperatures, and the Gidginbung zircons may have formed at even higher temperatures.

5.2. Oxygen and hafnium isotopes

All oxygen isotope data are listed in Electronic Annex Table EA3 and summarized in Table 1. Zircons from the Gidginbung deposit have a narrow range of $\delta^{18}O$ from 4.2 to 6.0‰ (average: 5.4±0.9‰, 2SD, n=17), and individual zircons are generally homogeneous in $^{18}O/^{16}O$, varying by less than 0.5‰ from core to rim. The oxygen isotope compositions of zircons from the Barmedman granite vary between 5.9 and 9.6‰ (average: 7.6±2.0‰, 2SD, n=17), much higher than the Gidginbung zircons.

The Hf isotope data for the Gidginbung zircons are reported in Electronic Annex Table EA4. Analyses (n=9) were mostly obtained from zircon rim domains showing concentric oscillatory zoning, with two analyses from large sector zoned cores. A single grain was large enough to support adjacent core and rim spots.

Irrespective of grain morphology or microstructure, the Hf isotope composition of the Gidginbung zircons shows limited variability. Initial $^{176}Hf/^{177}Hf$ values cluster between 0.282682±0.000011 and 0.282722±0.000013 (2SE) (average: 0.282697±0.000030, 2SD), the corresponding $\varepsilon_{Hf}(t=435$ Ma) values being 6.4±0.9 and 7.8±0.9 (2SE). This range slightly exceeds that shown by zircon standards, but is commensurate with the lower average internal precision of the Gidginbung analyses and testifies to the Hf isotope homogeneity of the zircon-crystallizing medium. Five grains in the Barmedman granite were analyzed for comparative purposes. These showed much greater
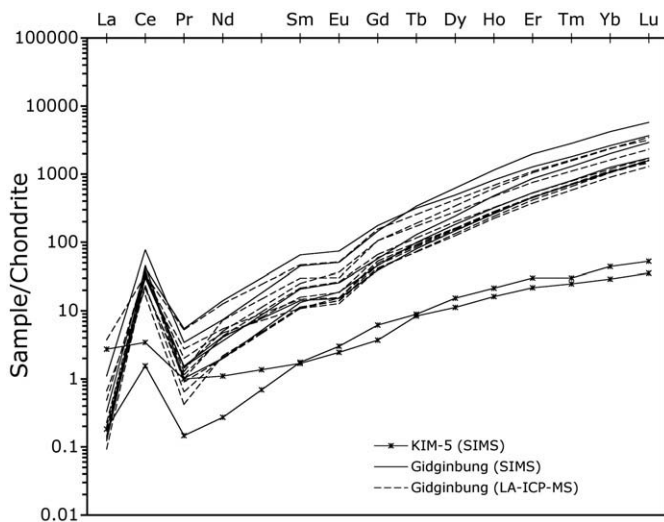
Fig. 2. Chondrite-normalized REE patterns for zircons (individual analysis) from the Gidginbung deposit analyzed by SIMS and LA-ICP-MS, compared with kimberlite zircon KIM-5. The C1 chondrite values are taken from McDonough and Sun (1995).

variability in $\varepsilon_{Hf}(t=370$ Ma), from 5.1±1.1 to 8.4±0.8 (2SE), which is consistent with previously published data (Kemp et al., 2005a).

6. Discussion

6.1. Previous evidence for hydrothermal zircons at Gidginbung

As briefly mentioned above, evidence used to support the interpretation that the Gidginbung zircons are hydrothermal (Lawrie et al., 2007) includes: (1) Petrological studies indicate that zircons occur in the alteration assemblage and appear to increase in abundance from the marginal kaolinitic and illitic alteration zones to the core silica-sulphide and pyrophyllite alteration and mineralization zones. Within the main ore zone, coarse-grained euhedral zircons were interpreted to coexist in textural equilibrium with sulphides and alteration minerals such as rutile, barite, pyrophyllite, quartz, enargite (Cu_3AsS_4) and pyrite. (2) One zircon contained four fluid inclusions large enough to study. These small (<5 μm), two-phase aqueous inclusions with approximately 25–30 vol.% vapor homogenized from 308° to 340 °C, having a similar temperature range to those in gangue minerals from the Gidginbung deposit. (3) Nuclear microprobe imaging has shown that the Gidginbung zircons have trace element zonation patterns that match the oscillatory zoning observed in cathodoluminescence. Zoning is particularly evident in As, Sb, Th, Yb, U, Pb and Hf (e.g., Electronic Annex Fig. EA3). Moreover, pyrite in some of the zircons is interpreted to have been trapped during zircon crystallization. This led Lawrie et al. (2007) to conclude that the Gidginbung zircons grew after or contemporaneously with precipitation of these minerals from a hydrothermal fluid.

There is still some debate about the composition of the host rocks to the Gidginbung deposit. Lawrie et al. (2007) claim that the orebody is hosted in a sequence of interbedded epiclastic breccias and mudstones. However, Allibone et al. (1995) reported the presence of volcaniclastics ranging from relatively fine-grained sandstones to coarse matrix-supported volcanic conglomerates. The sandstones were interpreted as crystal-rich tuffs or epiclastic sediments. Thus, it is possible that the intensive alteration of these rocks by hydrothermal fluids has destroyed most of the original mineralogy except for some remaining residual zircons. As the shear zones represent the greatest reduction in rock volume it is reasonable to expect that they would also contain the highest concentration of residual minerals such as zircon.

Only four fluid inclusions in a single zircon from Gidginbung were studied by Lawrie et al. (2007). These inclusions homogenized over a temperature range from 308 to 340 °C and the variation in temperatures could be due to partial leakage of the inclusions. Despite the possibility of partial leakage, these homogenization temperatures may represent minimum entrapment temperatures. If the inclusions trapped an originally homogeneous fluid, then the actual trapping temperature cannot be constrained without additional information on the confining pressure at the time of trapping. Isolated or clustered low-salinity aqueous or mixed CO_2–H_2O inclusions in zircon igneous cores and/or metamorphic overgrowths from the Dabie-Sulu ultrahigh-pressure (UHP) eclogite and gneiss, eastern China have been reported, indicating the presence of pre- and/or syn-UHP metamoporphic fluids (Liu and Xu, 2004; Shen et al., 2005; Zhang et al., 2005). Therefore, the possibility that these inclusions were trapped at high temperatures and even magmatic conditions cannot be ruled out at this stage.

A re-examination of the zircons from Gidginbung shows that many of the pyrite, rutile, barite, quartz and probably strengite inclusions actually occur at the edge of the crystals (Fig. 3; Electronic Annex Table EA5). This indicates that these solid inclusions may have been trapped in the zircons subsequent to zircon crystallization or resorption. It should be noted that most of the solid inclusions are also known to occur in magmatic zircons elsewhere. The occurrence of quartz, rutile, anatase, barite and apatite as mineral inclusions has been reported in igneous zircon cores from orthogneiss (or metagranite) and/or paragneiss in the Dabie-Sulu ultrahigh-pressure metamorphic terranes, eastern China (e.g., Liu et al., 2001). Pyrite
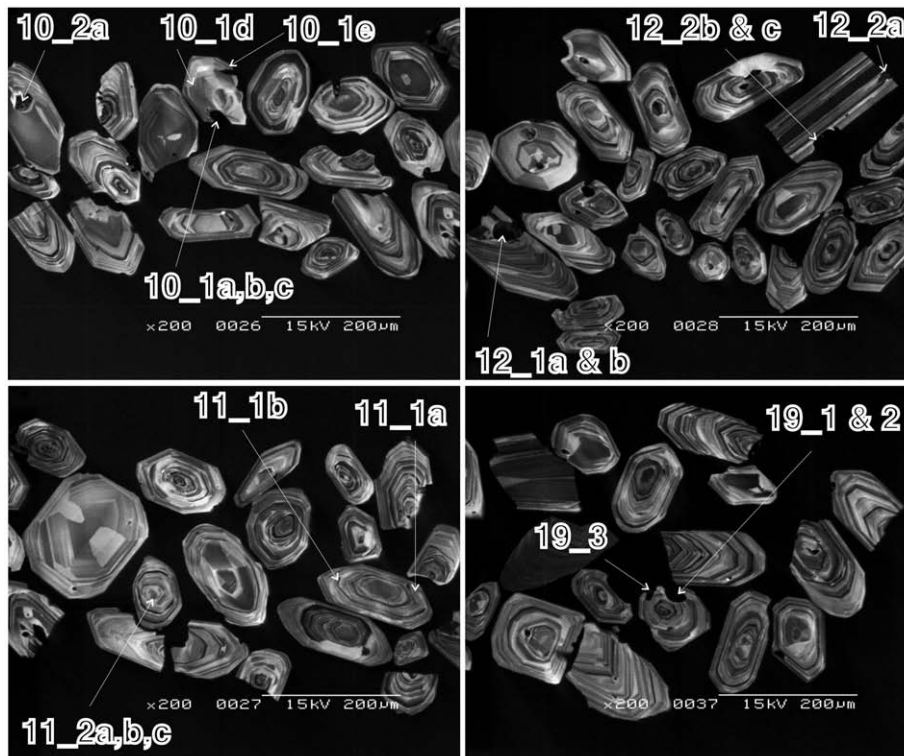

Fig. 3. The mode of occurrence of mineral inclusions in zircons identified by laser Raman microprobe on cathodoluminescence images. Note: (10_1a, c, d, 11_2a and c, 12_1a, 12_2b and c, 19_1 and 3), pyrite; (10_1b and e, 11_2b) quartz; (10_2a) strengite; (11_1a, 12_1b) rutile; (11_1b) anatase; (12_2a, 19_2) barite; see also Electronic Annex Table EA5.

can be stable at temperatures up to 743 °C (Fleet, 2006 and references therein). Considering the similarity of CL patterns to other zircons, we propose that those zircons containing pyrite in the core (Fig. 3) can also be of igneous origin, although the possibility that the zircons may contain domains of hydrothermal origin cannot be completely ruled out. Only one of the zircons containing strengite (#10B) which is probably transferred from precursor apatite in an intracrystalline fracture was analyzed by LA-ICP-MS, and the REE data are discussed below.

The presence of chemical zoning in zircons from Gidginbung has been reported by Lawrie et al. (2007; see Fig. 5 therein) with the concentration of minor and trace elements decreasing towards the rim of the crystals. Zoning is particularly evident for Fe, As and Sb and suggests that the sulfides and chalcophile metals may have been partitioned into a separate fluid or sulfide melt from silicate melt during the initial stages of magmatic fractionation as seen in porphyry ore deposits (e.g., Halter et al., 2002). Thus, some of the sulfides may have been incorporated into these zircons during the rhythmic accretion of zircon onto the core of the crystals as indicated by the oscillatory zoning in the cathodoluminescence images (Fig. 3 of Lawrie et al., 2007). The possible kinetically retarded substitution of these trace elements into the zircon lattice from highly-ordered silicate melt can be expressed as: As^{3+} (or Sb^{3+})$+P^{5+}=Zr^{4+}+Si^{4+}$.

6.2. Comparison with other hydrothermal zircons

Several case studies (Hoskin, 2005; Pettke et al., 2005; Rimsa et al., 2007; Kebede et al., 2007; Pelleter et al., 2007) have demonstrated that hydrothermal zircons display a distinct REE distribution pattern from the associated magmatic zircons. For comparison, we compiled some of the previously published trace elements (particularly, REE) data for both magmatic and hydrothermal zircons from various igneous rocks from the Lachlan Orogen and adjacent New England Orogen, to further constrain the origin of Gidginbung zircons.

The igneous rocks include: Middledale gabbroic diorite (Temora-1 and 2: 416.8±2.6 Ma, 2SD), Boggy Plain Zoned Pluton (I-type), Blind gabbro (I-type; Hine et al., 1978; 417 Ma; W.J. Collins, pers. comm.), Berridale adamellite (S-type; 435±5 Ma), Kosciusko tonalite (i.e., Jindabyne tonalite from the Kosciusko Batholith; S-type; 418±4 Ma) from the Lachlan Orogen, and Dundee rhyodacite ignimbrite (I-type; 257.6±2.5 Ma), Mole Granite (A-type; ~248 Ma) from the New England Orogen (Hoskin and Ireland, 2000; Hoskin et al., 2000; Black et al., 2004; Hoskin, 2005; Pettke et al., 2005; Schaltegger et al., 2005; Belousova et al., 2006). The classification of I- and S-type granite, correlates to the distinction between metaluminous and strongly peraluminous granite (Chappell and White, 1974, 2001), while peralkaline granite is regarded as being A-type.

Previously published data for other zircons of inferred hydrothermal origin, including those from a migmatitic granite from the Tjärnesjö intrusion, southwest Sweden; from albitized banded rhyolitic metatuffites and albitites from the Tamlalt-Menhouhou gold deposit, Morocco; and from a zircon microvein in peralkaline granitic gneiss, western Ethiopia, are also taken for comparison from the literature (Rimsa et al., 2007; Pelleter et al., 2007; Kebede et al., 2007). The chondrite-normalized REE patterns of zircons from the Gidginbung deposit (Fig. 4) are distinct from those of magmatic zircons from the Blind gabbro, Berridale adamellite, Kosciusko tonalite, Dundee rhyodacite ignimbrite and Mole Granite (Hoskin and Ireland, 2000; Hoskin et al., 2000; Pettke et al., 2005; Belousova et al., 2006).

The Gidginbung zircons share similar REE distribution patterns to magmatic zircons from the nearby Middledale Gabbroic Diorite (Black et al., 2004) and from the Boggy Plain Zoned Pluton including diorite, granodiorite, adamellite and aplite (Hoskin and Ireland, 2000; Hoskin et al., 2000; Hoskin, 2005), and also to hydrothermal zircons from the Mole Granite (Yankee Lodes; Pettke et al., 2005) and from the albitized banded rhyolitic metatuffites and albitites of the Tamlalt-
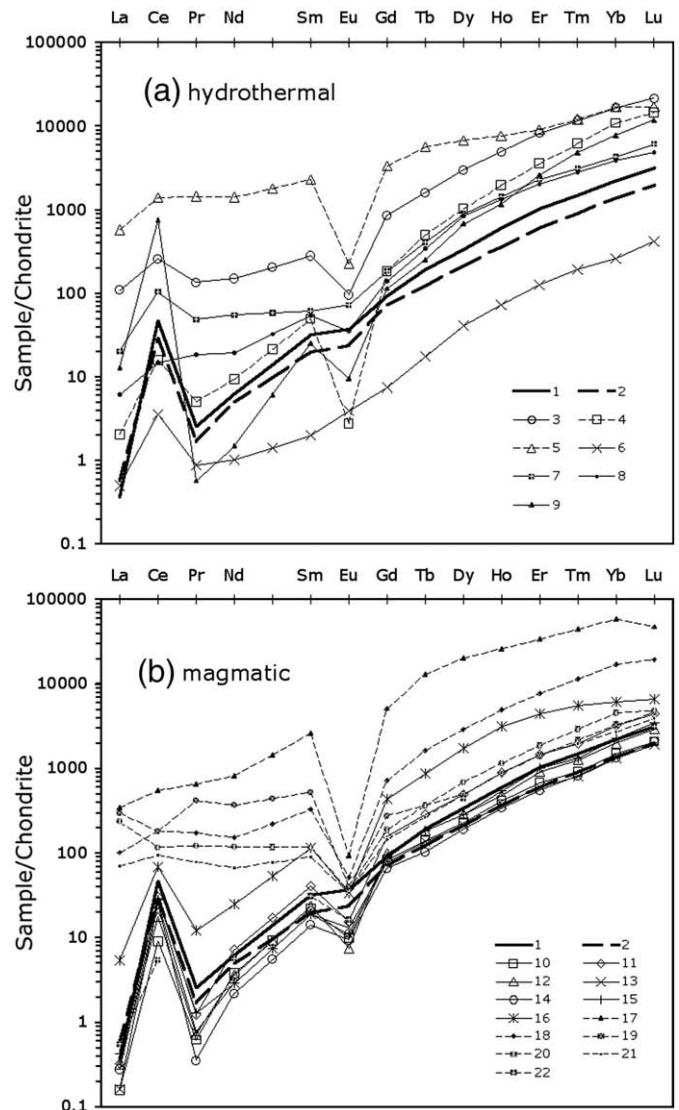

Fig. 4. Comparison of chondrite-normalized REE patterns for zircons from the Gidginbung deposit (heavy lines) with so-called *hydrothermal* zircons reported elsewhere in (a) and *magmatic* zircons from intrusions from the Lachlan Orogen and adjacent New England Orogen in (b). All are average REE values, analyzed by SIMS (solid line) and LA-ICP-MS (dashed line). The C1 chondrite values are taken from McDonough and Sun (1995). Data sources: (1 and 2) Gidginbung zircons analyzed by SIMS and LA-ICP-MS, this study; zircons interpreted to be hydrothermal from: (3) the Boggy Plain Zoned Pluton aplite, Hoskin (2005); (4) Yankee Lodes and (5) Paradise Lode, Mole Granite, Pettke et al. (2005); (6) a migmatitic granite from the Tjärnesjö intrusion, southwest Sweden, Rimsa et al. (2007); (7) albitized banded rhyolitic metatuffites and (8) albitites from the Tamlalt-Menhouhou gold deposit, Morocco, Pelleter et al. (2007); (9) a microvein in peralkaline granitic gneiss, western Ethiopia, Kebede et al. (2007); and magmatic zircons from: (10) diorite, (11) outer and (12) inner granodiorite, (13) outer and (14) inter adamellite, and (15) aplite from the Boggy Plain Zoned Pluton, Hoskin et al. (2000); (16) the Blind gabbro, Hoskin and Ireland (2000); (17) Pheno and (18) Yankee Lodes, Mole Granite, Pettke et al. (2005); (19) the Kosciusko tonalite, (20) the Berridale adamellite and (21) the Dundee rhyodacite ignimbrite, Belousova et al. (2006); (22) the Middledale gabbroic diorite, Black et al. (2004).

Menhouhou gold deposit, Morocco (Pelleter et al., 2007). In this regard, REE patterns of hydrothermal and magmatic zircons are probably only distinctive in certain individual cases.

A further distinction between hydrothermal and magmatic zircons may be made in the discriminant diagrams as proposed by Hoskin (2005). In Fig. 5, all data points for the Gidginbung zircons fall within or near the field of magmatic zircons. $(Sm/La)_N$ values range from 12 to 198. The lowest value (12; zircon #10B which contains strengite) lies outside the typical range of magmatic zircon and suggests a trend
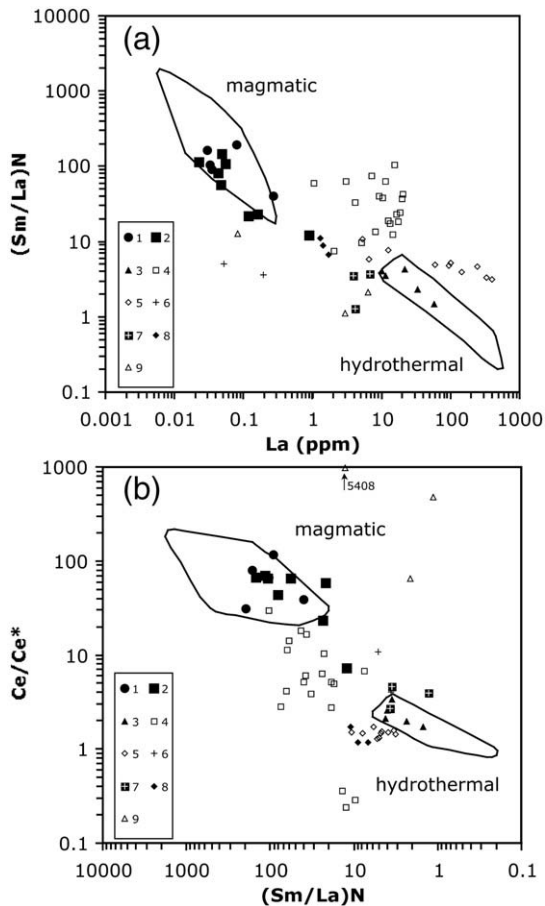
Fig. 5. Discriminant diagrams of (a) $(Sm/La)_N$ vs. La (ppm); (b) Ce/Ce^* vs. $(Sm/La)_N$ for zircons from the Gidginbung deposit (large solid symbols) compared to zircons from other areas that are interpreted to be hydrothermal in genesis. The two outlined areas in (a) and (b) are defined by magmatic and "hydrothermal zircons" from the Boggy Plain Zoned Pluton (Hoskin, 2005). $(Sm/La)_N = (Sm/0.148)/(La/0.237)$, $Ce/Ce^* = (Ce/0.613)/SQRT((La/0.237)^*(Pr/0.0928))$; all chondrite values are taken from McDonough and Sun (1995). Data sources: (1 and 2) Gidginbung zircons analyzed by SIMS and LA-ICP-MS, this study; zircons interpreted to be hydrothermal from: (3) the Boggy Plain Zoned Pluton aplite, Hoskin (2005); (4) Yankee Lodes and (5) Paradise Lode, Mole Granite, Pettke et al. (2005); (6) a migmatitic granite from the Tjärnesjö intrusion, southwest Sweden, Rimsa et al. (2007); (7) albitized banded rhyolitic metatuffites, and (8) albitites from the Tamlalt-Menhouhou gold deposit, Morocco, Pelleter et al. (2007); (9) a microvein in peralkaline granitic gneiss, western Ethiopia, Kebede et al. (2007).

towards hydrothermal compositions (Fig. 5a). Similarly, the Gidginbung zircons are characterized by a prominent positive Ce anomaly ranging from 7 to 120 with most data plotting within the magmatic field except for the lowest value (7) for the same zircon (#10B) above. This again suggests transitional compositions between magmatic and hydrothermal zircon (Fig. 5b), however, the geological meaning remains uncertain. Only a few data points for hydrothermal zircons reported elsewhere fall within the field of hydrothermal zircons from Boggy Plain Zoned Pluton aplite, which suggests that the so-called discriminants are not particularly robust.

Another pronounced difference is that the zircons from Gidginbung have a very small negative Eu anomaly (Eu/Eu*, $(Eu)_N/SQRT(Sm·Gd)_N$, ranges from 0.54 to 0.76). Th/U ratios are between 0.32 and 0.70 as commonly seen in magmatic zircons, while hydrothermal zircons frequently have more extreme values. However, the zircons interpreted to be hydrothermal from the Boggy Plain Zoned Pluton aplite and the Mole Granite (Fig. 6) have variable Th/U rations (0.05 to 0.82) and thus it appears that the Th/U ratio is more variable than proposed by Hoskin and Schaltegger (2003), <0.1, and is an unreliable indicator of hydrothermal zircon. Recent studies (e.g., Harley et al., 2007, and references therein; see also Schulz et al., 2006) indicate that

the Th/U ratio in zircon mainly reflects protolith characteristics or the local chemical environment of formation, even including the reservoir from which fluids were derived.

The average Nb/Hf in the Gidginbung zircons is $3.4\pm2.2\times10^{-4}$ (2SD, $n = 10$; Electronic Annex Table EA2). It is comparable to zircons from I-type granites of the Lachlan Orogen (e.g., the Cobargo and Jindabyne suites), which have a Nb/Hf ratio below 2×10^{-4}, one or two orders of magnitude lower than those from typical intra-plate, A-type granites (highly variable, $>3\times10^{-4}$; Hawkesworth and Kemp, 2006).

6.3. Zircon crystallization temperature

Crystallization temperature, if accurately known, is a useful parameter for distinguishing hydrothermal zircon (commonly crystallizing below 500 °C) from magmatic zircon ($>\sim600$ °C). The Ti content in zircons from other hydrothermal and/or magmatic zircons from igneous rocks of the Lachlan Orogen and adjacent New England Orogen has also been previously analyzed by LA-ICP-MS (Hoskin and Ireland, 2000; Hoskin et al., 2000; Hoskin, 2005; Pettke et al., 2005). Compared to this study, most of the previous LA-ICP-MS analyses gave relatively high Ti content in zircon, corresponding to high apparent temperatures. Apparent temperatures for hydrothermal zircons from the Boggy Plain Zoned Pluton aplite and the Mole Granite are <952° to 1101 °C and <698° to 988 °C, respectively, unreasonably higher than the associated magmatic zircons in the former case (757° to 956 °C). All of these Ti-data are plotted against Th/U in Fig. 6. To interpret these high apparent temperatures, there are several possibilities: (1) either background levels in Ti for LA-ICP-MS were high or Ti-rich mineral inclusions were analyzed by LA-ICP-MS; (2) a new calibration of the Ti-in-zircon thermometry (Ferry and Watson, 2007) should be applied and multiple variables such as activities of TiO_2 and SiO_2 and pressure and other factors need to be addressed (Fu et al., 2008), which is not the case for the Gidginbung zircons as discussed above. Comparing the LA-ICP-MS data to the SIMS data for the Gidginbung zircons rules out the first possibility. Therefore, considering that the Ti-in-zircon temperatures are commonly lower than predicted crystallization temperatures for igneous zircons (Fu et al., 2008), we conclude that these hydrothermal zircons do not record significantly lower temperatures than magmatic zircons.

If the initial whole-rock composition of the host igneous rock is known, zircon saturation temperatures can be estimated using the experimental calibration of Watson and Harrison (1983) within the compositional range $M = (Na+K+2Ca)/(Al·Si)$ from 0.9 to 1.9. The results of some of the previously analyzed samples in the Lachlan Orogen are summarized below. It is known that the zirconium content in the
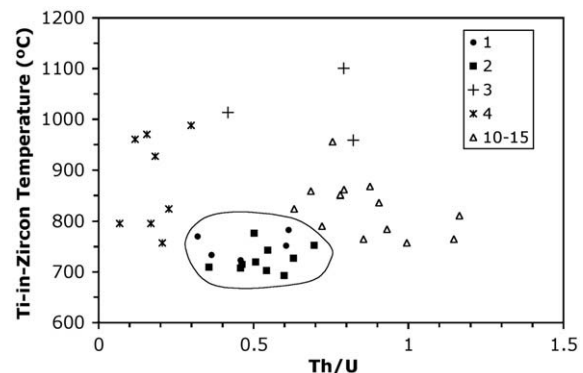

Fig. 6. Apparent Ti-in-zircon temperature vs. Th/U for the Gidginbung Au deposit (solid symbols), analyzed by (1) SIMS and (2) LA-ICP-MS. Th/U varies from 0.3 to 0.7 (L.P. Black, Geoscience Australia, unpublished data). Data sources: zircons interpreted to be hydrothermal from: (3) hydrothermal zircons from the Boggy Plain Zoned Pluton aplite, Hoskin (2005); and (4) Yankee Lodes, Mole Granite, Pettke et al. (2005); (10–15) magmatic zircons from the Boggy Plain Zoned Pluton (diorite, granodiorite, adamellite and aplite; Hoskin and Ireland (2000) and Hoskin et al. (2000), all analyzed by LA-ICP-MS.

Boggy Plain Zoned Pluton and other I-type granites from the Lachlan Orogen ranges between ~30 and 300 ppm (e.g., Chappell et al., 2004, and references therein; Wormald et al., 2004; Kemp et al., 2005b), and up to 500 ppm for A-type granites (e.g., King et al., 2001). In this regard, the estimated zircon saturation temperatures are 738° to 762 °C, for adamellite of the Boggy Plain Zoned Pluton (Wyborn, 1983; after Hoskin, 2000); and 795° to 845 °C, for the Barmedman Suite (Wormald et al., 2004). Elsewhere, King et al. (2001) estimated zircon saturation temperatures of A-type granites from the Wangrah Suite to be between 763° and 894 °C. The zircon saturation temperature was also calculated (Kemp et al., 2005b) to be 766 °C, for the Cobargo Monzogranite; 785° and 809 °C, for the Why Worry and Pretty Point Tonalites (Why Worry Suite); and 715° and 743 °C, for the Round Flat Tonalite (Jindabyne Suite). As indicated by Kemp et al. (2005b), some igneous rock suites (e.g., the Why Worry and Cobargo Suites) are characterized by decreasing Zr contents with increasing SiO_2, however, zircon saturation temperatures based on whole rock analyses may not be a reliable measure of the temperature at which zircon saturation occurred due to restite-melt unmixing of meta-igneous protolith (Chappell et al., 2004) or differentiation of the host magma (Kemp et al., 2005b). Chappell et al. (2004) further concluded that, "zircon saturation temperature calculated for such suites can be used to assess whether or not the rock compositions are those of melts".

Again, if the initial whole-rock composition of the host igneous rock is known, for those igneous rocks with a M value out of the experimental range (e.g., mafic-intermediate rocks), the MELTs algorithm (Ghiorso and Sack, 1995; Asimow and Ghiorso, 1998) can be employed to estimate crystallization temperature of the melt. The liquidus temperature estimated by MELTs for the Middledale Gabbroic Diorite (Temora-1 and 2: M=3.0 or 2.6; Black et al., 2004) is ~1100° to 1200 °C at water contents between 0.2 and 4.0 wt.% (Fu et al., 2008), while the predicted solidus temperature (750° or 695 °C) is comparable to the apparent Ti-in-zircon temperatures (692° to 782 °C) for the Gidginbung deposit. This is also the case for the Boggy Plain Zoned Pluton (Wyborn, 1983; after Hoskin, 2000; Electronic Annex Tables EA6 and 7): The calculated crystallization temperature is ~810 °C (diorite, 10 to 15% melt residue, water contents from 0.2 to 4.0 wt.%); or 730 °C (granodiorite, solidus, 0.2 wt.% H_2O). By contrast, the predicted solidus at water contents between 0.2 and 1.0 wt.% is ~880 °C, for an Ordovician shoshonitic monzodiorite from Temora (M=4.3; Sample 79 of Wormald et al., 2004). Therefore, the high Ti-temperatures for zircons from the Gidginbung deposit (comparable to the calculated zircon saturation temperature or crystallization temperature of melt in the region) do not support the hypothesis that the zircons have formed from low-temperature, hydrothermal fluids responsible for gold mineralization.

6.4. Isotopic signature of the parent rock

If the Gidginbung zircons crystallized in equilibrium with an ore-mineralizing fluid at 350°~700 °C, the fluid should have a $\delta^{18}O$ value of 6.4 to 7.5‰ ($\Delta^{18}O_{Zrc-H_2O}$=−1.0‰ at T=350 °C or −2.1‰ at 700 °C; Clayton et al., 1972; Valley et al., 2003), distinctive from modern meteoric water. It is well known that D/H and $^{18}O/^{16}O$ ratios of meteoric water depend on geographic location, and that both generally decrease from the equatorial region to the polar regions (Hoefs, 2004). The southeastern Australian continent was located at low latitudes, 30°N to 10°S, between ~450 and 420 Ma (Li and Powell, 2001), and modern meteoric water at the same latitudes has a negative $\delta^{18}O$ value (IAEA, 1981). In this regard, the fluid responsible for zircon growth is unlikely to be dominantly meteoric water, and it is typical of primary magmatic water (Hoefs, 2004). Allibone et al. (1995) reported that $\delta^{18}O$ for quartz separates from fiber veins (some of them cutting the silica-pyrite alteration) from the Gidginbung deposit varies from 14.2 to 17.0‰ (average: 15.6±1.9, 2SD, n=9), slightly lower than that for the silica-pyrite alteration (bulk analysis), 15.7 to 17.9‰ (16.7±2.2,

n=5). Isotopic compositions of fluids at equilibrium with quartz ($\Delta^{18}O_{Qtz-H_2O}$=5.8‰ at T=350 °C or 0.7‰ at 700 °C; Clayton et al., 1972) were estimated to be 8.4 to 11.2‰ (average: 9.8‰) at 350 °C, or 13.5 to 16.3‰ (average: 14.9‰) at 700 °C. Combined with hydrogen isotope compositions of various alteration zones at Gidginbung, Allibone et al. (1995) concluded that mineralization was associated with a predominantly magma-derived fluid, possibly with some input of meteoric water along the margins of the hydrothermal system. The large measured oxygen isotopic fractionation between quartz and zircon (average: ~10‰) does not support the suggestion that the minerals formed together at 350 °C or above. In other words, both zircon and quartz must have formed by different processes and/or from different reservoirs.

The host rock of the Gidginbung zircons has been extensively hydrothermally altered. However, it is possible to estimate the oxygen isotopic composition of the host rock of the Gidginbung zircons, based on the empirical calibration of Valley et al. (2005), if the host rock is assumed to be of igneous origin. The oxygen isotopic fractionation between zircon and the host whole-rock, $\Delta^{18}O$ (Zrc−WR), is approximately a linear function of SiO_2 (wt.%) for igneous rocks at magmatic temperatures: $\Delta^{18}O$ (Zrc−WR)=$\delta^{18}O$ (Zrc)−$\delta^{18}O$ (WR)≈−0.0612×(wt.% SiO_2)+2.5. The $\Delta^{18}O$ (Zrc−WR) value varies from ~−0.5‰ for mafic rocks (e.g., 49 wt.% SiO_2) to ~−2.1‰ for granitic rocks (e.g., 75 wt.% SiO_2). Therefore, the parent host rock of the Gidginbung zircons ($\delta^{18}O$ (Zrc) ~5.4‰) likely had a $\delta^{18}O$ (WR) value between ~5.9‰ and ~7.5‰, much lower than typical S-type granites (whole-rock $\delta^{18}O$>10‰: O'Neil and Chappell, 1977; Chappell and White, 2001; and mostly between 63 and 78 wt.% SiO_2: Chappell et al., 2004) from the Lachlan Orogen. Zircons from the Barmedman Suite have a $\delta^{18}O$ value of 7.6‰, implying a higher whole-rock $\delta^{18}O$ value, approximately 9.7‰ (SiO_2= 75 wt.% for the rock; Wormald et al., 2004). Worldwide, S-type granites commonly have higher $\delta^{18}O_{WR}$, 10 to 14‰, than I-type granites, 6 to 10‰ (e.g., O'Neil and Chappell, 1977; Eiler, 2001). Therefore, the oxygen isotopic composition indicates that the parent rock of the Gidginbung zircons, if it is igneous, is unlikely to be an S-type granite and this is also supported by the Hf isotope data.

The Gidginbung zircons have a lower $\delta^{18}O$ value, ~5.4‰, (but older U–Pb age) than those from other igneous rocks in the same area including the Middledale gabbroic diorite (Temora-1 and 2: ~8.1‰; Black et al., 2004; Kemp et al., 2007; or 8.2‰; Ickert et al., 2008), and the Barmedman I-type granite (~7.6‰), as listed in Table 1 and shown in Fig. 7. Zircons from the Narraburra peralkaline rocks have $\delta^{18}O$ values, ranging from 4.5 to 5.5‰ (A.I.S. Kemp, unpublished data), consistent with a typical zircon $\delta^{18}O$ value of <6‰ for A-type granites elsewhere (Valley et al., 2005). At a regional scale, zircons from the Blind gabbro (417 Ma; W.J. Collins, pers. comm.), tonalite and syn-plutonic basalt from the Why Worry Suite (~400 Ma), Round Flat tonalite from the Jindabyne Suite (~415 Ma), and mafic to felsic granite (i.e., diorite, tonalite and granite) from the Cobargo Suite (~390 Ma) have a relatively high average $\delta^{18}O$ value (6.50±1.49 to 8.13±1.29‰, 2SD) and a wide range from 4.8 to 9.4‰ (Kemp et al., 2007; Table 1 and Fig. 7). Kemp et al. (2006b) also reported zircon $\delta^{18}O$ data for ~430 Ma cordierite-bearing granites (S-type) from the Lachlan Orogen: 9.1± 1.0‰ (2SD, n=17), for Hawkins dacite (431±8 Ma); 8.4±1.2‰ (n=10), for Cootralantra granodiorite (428±10 Ma), whereas zircons from Arable granodiorite (S-type, ~428 Ma) yield a $\delta^{18}O$ value of 9.5±1.0‰ (n=14; A.I.S. Kemp, unpublished data). By by also using in-situ technique (SHRIMP II), Ickert et al. (2008) reported zircon $\delta^{18}O$ data for some other igneous rocks in the region: 5.6±0.6‰ (2SD; n=11), Blind gabbro, slightly lower than but overlapping within error that (6.69± 0.92‰) reported by Kemp et al. (2007; see Table 1); 6.6±0.8‰ (n=13), Jindabyne tonalite, whereas the zircon $\delta^{18}O$ values for Jillamatong granodiorite (S-type, also from the Kosciusko Batholith) vary from 8.2 to 10.2‰ (average: 9.1‰, n=11). Therefore, only the Gidginbung zircons (and some, if not all, from the Blind gabbro) have an entirely mantle-like oxygen isotope signature.
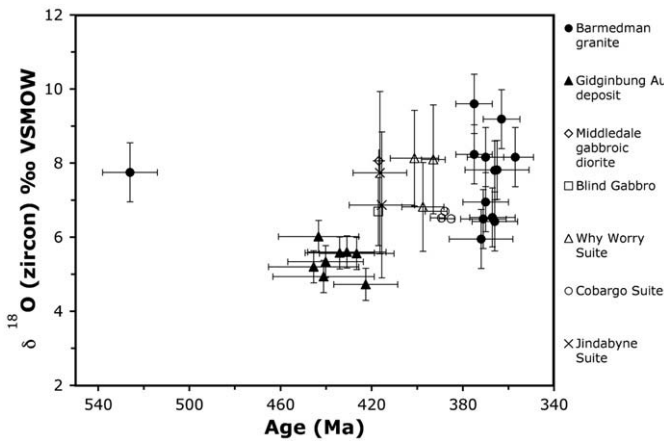
Fig. 7. Oxygen isotope ratios of zircon against U–Pb age for the Gidginbung Au deposit and adjacent Barmedman granite. Solid symbols represent individual analyses, whereas open symbols and cross stand for average values, all analyzed by SIMS, except the Middledale Gabbroic Diorite (open diamond) by laser fluorination for $^{18}O/^{16}O$ and by ID-TIMS for U–Pb age (Table 1). Data sources: average U–Pb age (416.8±2.6, 2SD; ID-TIMS) and $\delta^{18}O$ value (8.06±0.30, 2SD, n=6; laserprobe) for Temora-1 and Temora-2 zircons from Middledale gabbroic diorite, Black et al. (2004). Error bar: ±2SD. No $\delta^{18}O$ data are available for the Narraburra peralkaline granite (375±8 Ma, 2SD; Kemp et al., 2005a). SHRIMP and ID-TIMS analyses of zircons from the Middledale gabbroic diorite, due to trace-element abundances, gave a slightly different U–Pb age (Black et al., 2003a,b, 2004): 416.6±2.0 Ma (2SD, weighted mean age) vs. 416.8±2.6 Ma (2SD), for Temora-1; 418.1±3.2 Ma (2SD) vs. 416.8±2.6 Ma (2SD), for Temora-2. The large error for ID-TIMS ages is derived from both spike-calibration and U decay-constant uncertainties (Black et al., 2003a, 2004), the value of 416.8±2.6 Ma (2SD) is selected here for comparison.

The Hf isotope compositions of the Gidginbung zircons in themselves cannot diagnose a hydrothermal versus magmatic origin, given the potentially large range of $^{176}Hf/^{177}Hf$ of hydrothermal fluids (which depend on the ultimate source of the fluids and the reservoirs with which this fluid subsequently interacts). Nevertheless, given the inferred super-solidus crystallization temperatures, these data are perhaps more easily interpreted in a magmatic context. The Hf isotope compositions of the Gidginbung zircons are distinctly more radiogenic than those of coeval S-type granites of the Lachlan Orogen ($\varepsilon_{Hf}(t)$: −2 to −13, Kemp et al., 2006b), but overlap with those of a slightly older (440 Ma) monzodiorite intrusion from the adjacent Macquarie Arc ($\varepsilon_{Hf}(t)$: +11 to +6). The $\varepsilon_{Hf}(t)$ values of the Macquarie Arc plutons decrease systematically from 484 Ma to 439 Ma (Kemp et al., 2005a). These data imply that the isotope composition of the crystallizing medium for the Gidginbung zircons reflects the terminal stages in the evolution of the Macquarie Arc, immediately prior to arc shutoff, crustal thickening and S-type granite emplacement associated with the Benambran orogeny (440–430 Ma). The Hf and O isotope compositions of the Gidginbung zircons can be reconciled by either derivation from subduction-fertilized mantle, or from older meta-igneous arc basement (or various combinations thereof). Lastly, we note that the similarity in $\varepsilon_{Hf}(t)$ of the Gidginbung zircons and those from the nearby Middledale gabbroic diorite (417 Ma, $\varepsilon_{Hf}(t)=+3$ to +8) suggest that the precursor magmas to these intrusions could well have been derived from the same lithospheric reservoir.

7. Conclusions

Our results indicate that the zircons from the Gidginbung Au–Ag–(Cu) deposit are characterized by REE patterns with a steep slope from La to Lu and a significantly positive Ce-anomaly and relatively negative Eu-anomaly, similar to magmatic zircons for some igneous rocks (e.g., the Middledale Gabbroic Diorite and the Boggy Plain Zoned Pluton) in the Lachlan Orogen. The high Ti-in-zircon temperatures and mantle-like oxygen and hafnium isotope compositions for the Gidginbung zircons show that they share the same chemical and isotopic signature as magmatic zircons in the region. We conclude that

the zircons from the Gidginbung gold deposit are indistinguishable from magmatic zircons in regards to morphology, CL patterns, and chemical and isotopic signatures. The large measured oxygen isotopic fractionation between quartz and zircon indicates that the minerals did not form by the same process or from the same reservoir at 350 °C or above. Furthermore, pyrite inclusions reported for a few zircons are interpreted to have been trapped at relatively high temperatures during zircon crystallization. Therefore, the Gidginbung zircons do not provide unequivocal evidence of a hydrothermal origin, especially at low temperatures, and isotopic signatures support the hypothesis that the zircons crystallized in magmas.

Appendix A. Supplementary data

Supplementary data associated with this article can be found, in the online version, at doi:10.1016/j.chemgeo.2008.10.035.

References

Allibone, A.H., Cordery, G.R., Morrison, G.W., Jaireth, S., Lindhorst, J.W., 1995. Synchronous advanced argillic alteration and deformation in a shear zone-hosted magmatic hydrothermal Au–Ag deposit at the Temora (Gidginbung) Mine, New South Wales. Economic Geology 90, 1570–1603.

Asimow, P.D., Ghiorso, M.S., 1998. Algorithmic modifications extending MELTS to calculate subsolidus phase relations. American Mineralogist 83, 1127–1132.

Bacchin, M., Duggan, M., Glen, R., Gunn, P., Lawrie, K., Lyons, P., Mackey, T., Raphael, N., Raymond, O., Robson, D., Sherwin, L., 1999. Cootamundra, Interpreted Geology Based on Geophysics and Previous Geological Mapping (1:250 000 Scale Map). Australian Geological Survey Organisation, Canberra and Geological Survey of New South Wales, Sydney.

Belousova, E.A., Griffin, W.L., O'Reilly, S.Y., 2006. Zircon crystal morphology, trace element signatures and Hf isotope composition as a tool for petrogenetic modeling: examples from eastern Australian granitoids. Journal of Petrology 47, 329–353.

Black, L.P., Kamo, S.L., Allen, C.M., Aleinikoff, J.N., Davis, D.W., Korsch, R.J., Foudoulis, C., 2003a. TEMORA 1: a new zircon standard for Phanerozoic U–Pb geochronology. Chemical Geology 200, 155–170.

Black, L.P., Kamo, S.L., Williams, I.S., Mundil, R., Davis, D.W., Korsch, R.J., Foudoulis, C., 2003b. The application of SHRIMP to Phanerozoic geochronology: a critical appraisal of four zircon standards. Chemical Geology 200, 171–188.

Black, L.P., Kamo, S.L., Allen, C.M., Davis, D.W., Aleinikoff, J.N., Valley, J.W., Mundil, R., Campbell, I.H., Korsch, R.J., Williams, I.S., Foudoulis, C., 2004. Improved $^{206}Pb/^{238}U$ microprobe geochronology by monitoring of a trace-element-related matrix effect: SHRIMP, ID-TIMS, ELA-ICP-MS and oxygen isotope documentation for a series of zircon standards. Chemical Geology 205, 115–140.

Chappell, B.W., White, A.J.R., 1974. Two contrasting granite types. Pacific Geology 8, 173–174.

Chappell, B.W., White, A.J.R., 2001. Two contrasting granite types: 25 years later. Australian Journal of Earth Sciences 48, 489–499.

Chappell, B.W., White, A.J.R., Williams, I.S., Wyborn, D., 2004. Low- and high-temperature granites. Transactions of the Royal Society of Edinburgh (Earth Science) 95, 125–140.

Claoue-Long, J.C., King, R.W., Kerrich, R., 1990. Archean hydrothermal zircon in the Abitibi Greenstone Belt: constraints on the timing of gold mineralization. Earth and Planetary Science Letters 98, 109–128.

Claoue-Long, J.C., King, R.W., Kerrich, R., 1992. Archean hydrothermal zircon in the Abitibi Greenstone Belt: constraints on the timing of gold mineralization—reply. Earth and Planetary Science Letters 109, 601–609.

Clayton, R.N., O'Neil, J.R., Mayeda, T.K., 1972. Oxygen isotope exchange between quartz and water. Journal of Geophysical Research 77, 3057–3067.

Cooke, D.R., Wilson, A.J., House, M.J., Wolfe, R.C., Walshe, J.L., Lickfold, V., Crawford, A.J., 2007. Alkalic porphyry Au–Cu and associated mineral deposits of the Ordovician to Early Silurian Macquarie Arc, New South Wales. Australian Journal of Earth Sciences 54, 445–463.

Corfu, F., Davis, D.W., 1991. Archean hydrothermal zircon in the Abitibi Greenstone Belt: constraints on the timing of gold mineralization—comment. Earth and Planetary Science Letters 104, 545–552.

Duggan, M., Lyons, P., 1999. Ocean-floor volcanism in the Lachlan Fold Belt: new evidence from the Wyalong area, New South Wales. AGSO Research Newsletter 31, 11–12.

Eiler, J.M., 2001. Oxygen isotope variations of basaltic lavas and upper mantle rocks. In: Valley, J.W., Cole, D.R. (Eds.), Stable Isotope Geochemistry. Reviews in Mineralogy and Geochemistry, vol. 43, pp. 319–364.

Ferry, J.M., Watson, E.B., 2007. New thermodynamic models and revised calibrations for the Ti-in-zircon and Zr-in-rutile thermometers. Contributions to Mineralogy and Petrology 154, 429–437.

Fleet, M.E., 2006. Phase equilibria at high temperatures. Reviews in Mineralogy and Geochemistry 61, 365–419.

Fu, B., Page, F.Z., Cavosie, A.J., Clechenko, C.C., Fournelle, J., Kita, N.T., Lackey, J.S., Wilde, S.A., Valley, J.W., 2008. Ti-in-zircon thermometry: applications and limitations. Contributions to Mineralogy and Petrology 156, 197–215.

Ghiorso, M.S., Sack, R.O., 1995. Chemical mass transfer in magmatic processes. IV. A revised and internally consistent thermodynamic model for the interpolation and extrapolation of liquid–solid equilibria in magmatic systems at elevated temperatures and pressures. Contributions to Mineralogy and Petrology 119, 197–212.

Glen, R.A., Spencer, R., Willmore, A., David, V., Scott, R.J., 2007a. Junee-Narromine volcanic belt, Macquarie Arc, Lachlan Orogen, New South Wales: components and structure. Australian Journal of Earth Science 54, 215–241.

Glen, R.A., Crawford, A.J., Cooke, D.R., 2007b. Tectonic setting of porphyry Cu–Au mineralisation in the Ordovician–Early Silurian Macquarie Arc, Eastern Lachlan Orogen, New South Wales. Australian Journal of Earth Sciences 54, 465–479.

Gray, D.R., Foster, D.A., 2004. Tectonic evolution of the Lachlan Orogen, southeast Australia: historical review, data synthesis and modern perspectives. Australian Journal of Earth Sciences 51, 773–817.

Gustafson, L.B., Orquera, W., McWilliams, M., Castro, M., Olivares, O., Rojas, G., Maluenda, J., Mendez, M., 2001. Multiple centers of mineralization in the Indio Muerto District, El Salvador, Chile. Economic Geology 96, 325–350.

Halter, W.E., Pettke, T., Heinrich, C.A., 2002. The origin of Cu/Au ratios in porphyry-type ore deposits. Science 296, 1844–1846.

Harley, S.L., Kelly, N.M., Möller, A., 2007. Zircon behaviour and the thermal histories of mountain chains. Elements 3, 25–30.

Hawkesworth, C.J., Kemp, A.I.S., 2006. Using hafnium and oxygen isotopes in zircons to unravel the record of crustal evolution. Chemical Geology 226, 144–162.

Hine, R., Williams, I.S., Chappell, B.W., White, A.J.R., 1978. Contrasts between I- and S-type granitoids of the Kosciusko Batholith. Australian Journal of Earth Sciences 25, 219–234.

Hoefs, J., 2004. Stable Isotope Geochemistry, 5th Edition. Springer, Berlin. 340 pp.

Hoskin, P.W.O., 2000. Patterns of chaos: fractal statistics and the oscillatory chemistry of zircon. Geochimica et Cosmochimica Acta 64, 1905–1923.

Hoskin, P.W.O., 2005. Trace-element composition of hydrothermal zircon and the alteration of Hadean zircon from the Jack Hills, Australia. Geochimica et Cosmochimica Acta 69, 637–648.

Hoskin, P.W.O., Ireland, T.R., 2000. Rare earth element chemistry of zircon and its use as a provenance indicator. Geology 28, 627–630.

Hoskin, P.W.O., Kinny, P.D., Wyborn, D., Chappell, B.W., 2000. Identifying accessory mineral saturation during differentiation in granitoid magmas: an integrated approach. Journal of Petrology 41, 1365–1396.

Hoskin, P.W.O., Schaltegger, U., 2003. The composition of zircon and igneous and metamorphic petrogenesis. In: Hanchar, J.M., Hoskin, P.W.O. (Eds.), Zircon. Reviews in Mineralogy and Geochemistry, vol. 53, pp. 27–62.

Hough, M.A., Bierlein, F.P., Wilde, A.R., 2007. A review of the metallogeny and tectonics of the Lachlan Orogen. Mineralium Deposita 42, 435–448.

Hu, F.F., Fan, H.R., Yang, J.H., Wan, Y.S., Liu, D.Y., Zhai, M.G., Jin, C.W., 2004. Mineralizing age of the Rushan lode gold deposit in the Jiaodong Peninsula: SHRIMP U–Pb dating on hydrothermal zircon. Chinese Science Bulletin 49, 1629–1636.

IAEA, 1981. Deuterium and oxygen-18 in the water cycle. In: Gat, J.R., Gonfiantini, R. (Eds.), Stable Isotope Hydrology. IAEA Technical Report, vol. 210, p. 337.

Ickert, R.B., Hiess, J., Williams, I.S., Holden, P., Ireland, T.R., Lanc, P., Schram, N., Foster, J.J., Clement, S.W., 2008. Determining high precision, in situ, oxygen isotope ratios with a SHRIMP II: analyses of MPI-DING silicate-glass reference materials and zircon from contrasting granites. Chemical Geology 257, 114–128.

Jaques, A.L., Jaireth, S., Walshe, J.L., 2002. Mineral systems of Australia: an overview of resources, settings and processes. Australian Journal of Earth Sciences 49, 623–660.

Kebede, T., Horie, K., Hidaka, H., Terada, K., 2007. Zircon 'microvein' in peralkaline granitic gneiss, western Ethiopia: origin, SHRIMP U–Pb geochronology and trace element investigations. Chemical Geology 242, 76–102.

Kemp, A.I.S., Wormald, R.J., Whitehouse, M.J., Price, R.C., 2005a. Hf isotopes in zircon reveal contrasting sources and crystallization histories for alkaline to peralkaline granites of Temora, southeastern Australia. Geology 33, 797–800.

Kemp, A.I.S., Whitehouse, M.J., Hawkesworth, C.J., Alarcon, M.K., 2005b. A zircon U–Pb study of metaluminous (I-type) granites of the Lachlan Fold Belt, southeastern Australia: implications for the high/low temperature classification and magma differentiation processes. Contributions to Mineralogy and Petrology 150, 230–249.

Kemp, A.I.S., Hawkesworth, C.J., Paterson, B.A., Kinny, P.D., 2006a. Episodic growth of the Gondwana supercontinent from hafnium and oxygen isotopes in zircon. Nature 439, 580–583.

Kemp, A.I.S., Hawkesworth, C.J., Paterson, B.A., Foster, G.L., Kinny, P.D., Whitehouse, M.J., Maas, R., 2006b. Exploring the plutonic–volcanic link: a zircon U–Pb, Lu–Hf and O isotope study of paired volcanic and granitic units from southeastern Australia. Transactions of the Royal Society of Edinburgh. Earth Sciences 97, 337–355 (Published in 2008).

Kemp, A.I.S., Hawkesworth, C.J., Foster, G.L., Paterson, B.A., Woodhead, J.D., Hergt, J.M., Gray, C.M., Whitehouse, M.J., 2007. Magmatic and crustal differentiation history of granitic rocks from Hf–O isotopes in zircon. Science 315, 980–983.

Kerrich, R., King, R., 1993. Hydrothermal zircon and baddeleyite in Val–Dor Archean mesothermal gold deposits: characteristics, compositions, and fluid-inclusion properties, with implications for timing of primary gold mineralization. Canadian Journal of Earth Sciences 30, 2334–2351.

Kerrich, R., Kyser, T.K., 1994. 100 Ma timing paradox of Archean gold, Abitibi Greenstone Belt (Canada): new evidence from U–Pb and Pb–Pb evaporation ages of hydrothermal zircons. Geology 22, 1131–1134.

King, P.L., Chappell, B.W., Allen, C.M., White, A.J.R., 2001. Are A-type granites the high-temperature felsic granites? Evidence from fractionated granites of the Wangrag Suite. Australian Journal of Earth Sciences 48, 501–514.

Lawrie, K.C., Mernagh, T.P., Ellis, P., 1997a. Geology of the Gidginbung Au deposit, Lachlan Fold Belt, Central-West, NSW. Geological Society of Australia. SGEG Field Guide "Porphyry—Epithermal Deposits of the Lachlan Fold Belt", pp. 83–91.

Lawrie, K.C., Mernagh, T.P., Ellis, P., 1997b. Host rock control on localisation of the Gidginbung epithermal high sulfidation Au deposit. Geological Society of Australia, Abstracts, vol. 44, p. 45.

Lawrie, K.C., Mernagh, T.P., Ryan, C.G., van Achterbergh, E., Black, L.P., 2007. Chemical fingerprinting of hydrothermal zircons: an example from the Gidginbung high sulphidation Au–Ag–(Cu) deposit, Australia. Proceedings of the Geologists' Association 118, 37–46.

Li, Z.X., Powell, C.M., 2001. An outline of the palaeogeographic evolution of the Australasian region since the beginning of the Neoproterozoic. Earth-Science Reviews 53, 237–277.

Liu, F.-L., Xu, Z.-Q., 2004. Fluid inclusions hidden in coesite-bearing zircons in ultrahigh-pressure metamorphic rocks from southwestern Sulu terrane in eastern China. Chinese Science Bulletin 49, 396–404.

Liu, J.-B., Ye, K., Maruyama, S., Cong, B., Fan, H., 2001. Mineral inclusions in zircon from gneisses in the ultrahigh-pressure zone of the Dabie Mountains, China. Journal of Geology 109, 523–535.

McDonough, W.F., Sun, S.-s., 1995. The composition of the Earth. Chemical Geology 120, 223–253.

Norman, M.D., Griffin, W.L., Pearson, N.J., Garcia, M.O., O'Reilly, S.Y., 1998. Quantitative analysis of trace element abundances in glasses and minerals: a comparison of laser ablation ICPMS, solution ICPMS, proton microprobe, and electron microprobe data. Journal of Analytical Atomic Spectrometry 13, 477–482.

Norman, M.D., Pearson, N.J., Sharma, A., Griffin, W.L., 1996. Quantitative analysis of trace elements in geological materials by laser ablation ICPMS: Instrumental operating conditions and calibration values of NIST glasses. Geostandards Newsletter 20, 247–261.

O'Neil, J.R., Chappell, B.W., 1977. Oxygen and hydrogen isotope relations in the Berridale Batholith. Journal of the Geological Society of London, 133, 559–571.

Page, F.Z., Fu, B., Kita, N.T., Fournelle, J., Spicuzza, M.J., Schulze, D.J., Viljoen, F., Basei, M.A.S., Valley, J.W., 2007a. Zircons from kimberlite: new insights from oxygen isotopes, trace element, and Ti in zircon thermometry. Geochimica et Cosmochimica Acta 71, 3887–3903.

Page, F.Z., Ushikubo, T., Kita, N.T., Riciputi, L.R., Valley, J.W., 2007b. High precision oxygen isotope analysis of picogram samples reveals 2-μm gradients and slow diffusion in zircon. American Mineralogist 92, 1772–1775.

Pelleter, E., Cheilletz, A., Gasquet, D., Mouttaqi, A., Annich, M., El Hakourd, A., Deloule, E., Féraude, G., 2007. Hydrothermal zircons: a tool for ion microprobe U–Pb dating of gold mineralization (Tamlalt-Menhouhou gold deposit—Morocco). Chemical Geology 245, 135–161.

Perkins, C., Walshe, J.L., Morrison, G., 1995. Metallogenic episodes of the Tasman Fold Belt System, Eastern Australia. Economic Geology 90, 1443–1456.

Pettke, T., Audetat, A., Schaltegger, U., Heinrich, C.A., 2005. Magmatic-to-hydrothermal crystallization in the W–Sn mineralized Mole Granite (NSW, Australia)—Part II: evolving zircon and thorite trace element chemistry. Chemical Geology 220, 191–213.

Ramezani, J., Dunning, G.R., Wilson, M.R., 2000. Geologic setting, geochemistry of alteration, and U–Pb age of hydrothermal zircon from the Silurian Stog'er Tight gold prospect, Newfoundland Appalachians, Canada. Exploration and Mining Geology 9, 171–188.

Rimsa, A., Whitehouse, M.J., Johansson, L., Piazolo, S., 2007. Brittle fracturing and fracture healing of zircon: an integrated cathodoluminescence, EBSD, U–Th–Pb, and REE study. American Mineralogist 92, 1213–1224.

Rubin, J.N., Henry, C.D., Price, J.G., 1989. Hydrothermal zircons and zircon overgrowths, Sierra-Blanca Peaks, Texas. American Mineralogist 74, 865–869.

Rubin, J.N., Henry, C.D., Price, J.G., 1993. The mobility of zirconium and other immobile elements during hydrothermal alteration. Chemical Geology 110, 29–47.

Schaltegger, U., Pettke, T., Audétat, A., Reusser, E., Heinrich, C.A., 2005. Magmatic-to-hydrothermal crystallization in the W–Sn mineralized Mole Granite (NSW, Australia)—Part I: crystallization of zircon and REE-phosphates over three million years—a geochemical and U–Pb geochronological study. Chemical Geology 220, 215–235.

Schulz, B., Klemd, R., Braetz, H., 2006. Host rock compositional controls on zircon trace element signatures in metabasites from the Austroalpine basement. Geochimica et Cosmochimica Acta 70, 697–710.

Shen, K., Zhang, Z.-M., Sun, X.-M., Xu, L., 2005. Composition and evolution of ultrahigh-pressure metamorphic fluids: a fluid inclusion study of the drill cores from the main hole of Chinese Continental Scientific Drilling Program. Acta Petrologica Sinica 21, 489–504 (in Chinese with English abstract).

Valley, J.W., 2003. Oxygen isotopes in zircon. In: Hanchar, J.M., Hoskin, P.W.O. (Eds.), Zircon. Reviews in Mineralogy and Geochemistry, vol. 53, pp. 343–385.

Valley, J.W., Bindeman, I.N., Peck, W.H., 2003. Empirical calibration of oxygen isotope fractionation in zircon. Geochimica et Cosmochimica Acta 67, 3257–3266.

Valley, J.W., Lackey, J.S., Cavosie, A.J., Clechenko, C.C., Spicuzza, M.J., Basei, M.A.S., Bindeman, I.N., Ferreira, V.P., Sial, A.N., King, E.M., Peck, W.H., Sinha, A.K., Wei, C.S., 2005. 4.4 billion years of crustal maturation: oxygen isotope ratios of magmatic zircon. Contributions to Mineralogy and Petrology 150, 561–580.

Warren, A.Y.E., Gilligan, L.B., Raphael, N.M. 1995 Explanatory Notes, Cootamundra 1:250 000 Geological Sheet SI/55-11. Geological Survey of New South Wales, Sydney.

Watson, E.B., Harrison, T.M., 1983. Zircon saturation revisited: temperature and composition effects in a variety of crustal magma types. Earth and Planetary Science Letters 64, 295–304.

Watson, E.B., Harrison, T.M., 2005. Zircon thermometer reveals minimum melting conditions on earliest Earth. Science 308, 841–844.

Watson, E.B., Wark, D.A., Thomas, J.B., 2006. Crystallization thermometers for zircon and rutile. Contributions to Mineralogy and Petrology 151, 413–433.

Wilson, A.J., Cooke, D.R., Stein, H.J., Fanning, C.M., Holliday, J.R., Tedder, I.J., 2007. U–Pb and Re–Os geochronologic evidence for two alkalic porphyry ore-forming events in the Cadia district, New South Wales, Australia. Economic Geology 102, 3–26.

Woodhead, J.D., Hergt, J.M., 2005. A preliminary appraisal of seven natural zircon reference materials for in situ Hf isotope determination. Geostandards and Geoanalytical Research 29, 183–195.

Wormald, R.J., Price, R.C., 1988. Peralkaline granites near Temora, southern New South Wales: tectonic and petrologic implications. Australia Journal of Earth Sciences 35, 209–221.

Wormald, R.J., Price, R.C., Kemp, A.I.S., 2004. Geochemistry and Rb–Sr geochronology of the alkaline-peralkaline Narraburra Complex, central southern New South Wales: tectonic significance of Late Devonian granitic magmatism in the Lachlan Fold Belt. Australian Journal of Earth Sciences 51, 369–384.

Wyborn, D., 1983. Fractionation Processes in the Boggy Plain Zoned Pluton. Ph.D. thesis, Australian National University, Canberra, pp. 301.

Zhang, Z.-M., Shen, K., Xiao, Y.-L., van den Kerkhof, A.M., Hoefs, J., Liou, J.G., 2005. Fluid composition and evolution attending UHP metamorphism: study of fluid inclusions from drill cores, southern Sulu Belt, eastern China. International Geology Review 47, 297–309.